

# Synthetic gauge field in a single optomechanical resonator

Yuan Chen<sup>1,2,†</sup>, Yan-Lei Zhang<sup>1,2,†</sup>, Zhen Shen<sup>1,2,†</sup>, Chang-Ling Zou<sup>1,2</sup>, Guang-Can Guo<sup>1,2</sup>, and Chun-Hua Dong<sup>1,2</sup>  
<sup>1</sup>CAS Key Laboratory of Quantum Information, University of Science and Technology of China, Hefei 230026, P. R. China. and  
<sup>2</sup>CAS Center For Excellence in Quantum Information and Quantum Physics,  
 University of Science and Technology of China, Hefei, Anhui 230026, P. R. China.\*  
 (Dated: August 14, 2019)

Synthetic gauge fields have recently emerged [1, 2], arising in the context of quantum simulations, topological matter, and the protected transportation of excitations against defects. For example, an ultracold atom experiences a light-induced effective magnetic field when tunnelling in an optical lattice [3, 4], and offering a platform to simulate the quantum Hall effect and topological insulators. Similarly, the magnetic field associated with photon transport between sites has been demonstrated in a coupled resonator array [5, 6]. Here, we report the first experimental demonstration of a synthetic gauge field in the virtual dimension of bosonic modes in a single optomechanical resonator. By employing degenerate clockwise (CW) and counter-clockwise (CCW) optical modes and a mechanical mode, a controllable synthetic gauge field is realized by tuning the phase of the driving lasers. The non-reciprocal conversion between the three modes is realized for different synthetic magnetic fluxes. As a proof-of-principle demonstration, we also show the dynamics of the system under a fast-varying synthetic gauge field. Our demonstration not only provides a versatile and controllable platform for studying synthetic gauge fields in high dimensions but also enables an exploration of ultra-fast gauge field tuning with a large dynamic range, which is restricted for a magnetic field.

When charged particles move around in a closed loop, the enclosed magnetic flux  $\Phi_B$  induces a phase that leads to interesting topological phenomena in condensed matter physics. Non-trivial topological phases and topologically protected quantum states have been extensively explored for fundamental studies and quantum information processing. For uncharged particles or bosonic excitations, the essential effect of a gauge field can also be realized through a geometric phase [7], where a particle or excitation acquires a path-dependent phase by a carefully engineered Hamiltonian. Such a synthetic gauge field enables the simulation of quantum many-body physics with unprecedented precision and unconventional control of bosons [1, 2]. Thus, synthetic gauge fields have aroused tremendous research interest recently and have been realized in various systems, including ultracold atoms [3, 4], optical photons [5, 6, 8], phonons [9] and other bosonic

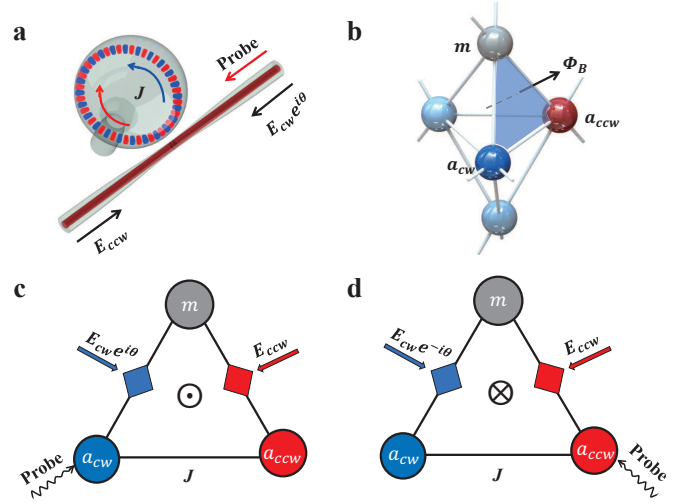


FIG. 1. Schematic illustration of a synthetic gauge field in an optomechanical resonator. **a** Two phase-related strong opposite propagating driving fields enhance the optomechanical coupling between a mechanical mode and the coupled optical modes inside a microcavity.  $E_{cw}$  ( $a_{cw}$ ) are the amplitudes of the clockwise (CW) and counter-clockwise (CCW) drives, and  $\theta$  is the phase difference between them. The CW and CCW modes are coupled through backscattering in the microresonator with the modal coupling strength of  $J$ . **b** Schematic of the CW and CCW optical modes coupling with the radial breathing mode. The synthetic magnetic flux  $\Phi_B$  arises from the phase-related driving fields.  $a_{cw}$ ,  $a_{ccw}$ , and  $m$  are the bosonic operators for the optical and mechanical modes, respectively. **c** Energy diagram for the mode conversion between the CW, and CCW optical modes and the breathing mode, where the probe is transferred from the CW (**c**) or CCW (**d**) direction. The accumulated phase in the CW to CCW optical mode conversion is reversed for the opposite propagating probe direction, which results in the non-reciprocal power transmission of the optical probe field.

quasi-particles [10, 11].

A synthetic gauge field is commonly realized in real space, where the excitation hops between sites and the phase accumulated for a closed loop path is not trivial. For photons, it has been realized in an artificial photonic microcavity array with engineered spatially dependent couplings between sites [5, 6, 8], while the hopping phase determined by the structural parameters is fixed and requires nanofabrication. Recently, a reconfigurable synthetic gauge field was proposed and realized in coupled resonators by employing parametric interactions [2, 12–

15]. For example, a closed loop of sites with a synthetic gauge field was realized by two coupled optomechanical resonators [14], where the appropriate spatially dependent hopping phases between sites were realized through external drives.

In this Letter, a synthetic gauge field is realized in a virtual dimension by exploring the natural optical and mechanical modes in a single spherical microresonator without the requirement of fabricating an array of identical microstructures. The effective magnetic flux can be precisely controlled by changing the phases of the external driving lasers. Additionally, such a synthetic gauge field can be arbitrarily tuned, offering the opportunity to study time-dependent gauge field dynamics. Benefiting from the great progress achieved in the coherent optomechanical interaction in microcavities and also the coherent nonlinear optical effects, our demonstration of the synthetic gauge field can be scaled up to larger dimensions but with full controllability, which is not available in real-space lattices. Therefore, exotic topological photonics and non-reciprocal quantum frequency conversion can be readily realized in a single microresonator.

The synthetic gauge field can be realized in a single optomechanical system, as illustrated in Fig. 1a. A single silica microsphere supports massive high-quality optical whispering gallery modes (WGMs) and mechanical modes [16, 17], by which the coherent conversion between the modes has been extensively studied in the context of optomechanics [18–21]. Therefore, by exploiting those modes as virtual dimensions, we can study an interesting model of bosonic lattices, as depicted in Fig. 1b, with each vertex node for the bosonic mode serving as a site and the edges corresponding to coherent hops between sites. For modes with non-degenerate frequencies, the coherent conversion between the modes can be stimulated by an external driving laser, which compensates for the energy difference between the modes. In the lattice, we can find the simplest closed loop of a triangle plaquette (blue surface in Fig. 1b), which consists of two optical modes and one mechanical mode. In a microsphere made of a non-magnetic material, the clockwise (CW) and counter-clockwise (CCW) optical modes are degenerate. However, the surface roughness and material defects induce backscattering of the photons [22], as described by an optical modal coupling strength  $J$  (Fig. 1a). Both the CW and CCW optical modes can optomechanically couple with the mechanical mode, while the CW (or CCW) photons can only couple with the phonon when there is an off-resonant intracavity field along the CW (or CCW) direction due to the conservation of momentum [23]. By introducing driving lasers in both the CW and CCW directions, coherent coupling between the optical modes and mechanical mode can be realized, with the hopping strength being proportional to the drives  $E_{\text{cw}}e^{i(\theta+\theta_0)}$  and  $E_{\text{ccw}}e^{i\theta_0}$ . Here,  $E_{\text{cw(ccw)}}$  is the amplitude of the drive, and  $\theta$  is the phase difference between

them. We know that the synthetic gauge field is from the phase difference, therefore we assume the common phase factor  $\theta_0 = 0$  for convenience.

Figures 1c-d provide a detailed model of the triangle plaquette, which is described by the Hamiltonian (see Supplementary Material for details)

$$H = Ja_{\text{cw}}a_{\text{ccw}}^\dagger + G_{\text{cw}}e^{i\theta}ma_{\text{cw}}^\dagger + G_{\text{ccw}}ma_{\text{ccw}}^\dagger + \text{H.c.}, \quad (1)$$

where  $m$ ,  $a_{\text{cw}}$  and  $a_{\text{ccw}}$  are the bosonic operators for the mechanical and optical modes, respectively.  $G_{\text{cw(ccw)}} \propto E_{\text{cw(ccw)}}$  is the stimulated photon-phonon coupling strength produced by red-sideband-detuned drives [18, 19]. The remaining phase  $\theta$  is gauge-independent and actually represents the phase gain by the bosonic excitations when circulating the plaquette. Such a phase  $\theta$  for bosonic excitations produces the Aharonov-Bohm effect for electrons, where electrons travel along a closed loop and gain a phase  $\theta = \frac{e}{\hbar c}\Phi_B$ . Here,  $\Phi_B$  is the magnetic flux enclosed by the loop, and  $e$ ,  $\hbar$  and  $c$  are the electron charge, reduced Planck's constant and the light velocity, respectively. Therefore, non-trivial effective gauge fields are synthesized for photons and phonons, while the flux  $\Phi_B$  can be controlled optically.

In our experiments, we fabricate a microsphere with a diameter of approximately  $32\mu\text{m}$ , which supports degenerated high-quality-factor WGMs near 780 nm (intrinsic optical linewidth of  $\kappa_0/2\pi = 5$  MHz, and a backscattering-induced modal coupling rate of  $J/2\pi = 5.3$  MHz). In the same resonator, the radial breathing mechanical mode has a frequency of  $\omega_m/2\pi = 98.72$  MHz and an optomechanical mode linewidth of  $\gamma_m/2\pi = 92$  kHz. In the experiments, both drives are generated from a laser passing through acoustic-optic modulators (AOMs), and the probe photons are generated by an electro-optic modulator (EOM). The phase  $\theta$  of the drives is precisely controlled through the relative phase delay between the radio-frequency (RF) signals driving the AOMs.

To verify the synthetic gauge field in our optomechanical resonator, we send probe laser to the optical CW mode. Comparing Figs. 1c and d, the model is symmetric under parity and time-reversal symmetry, i.e.,  $\theta \rightarrow -\theta$  and CW  $\rightarrow$  CCW. Therefore, the system behaviour for a probe input coupled to the optical CCW mode (Fig. 1d) is equivalent to the scheme in Fig. 1c by flipping the phase of the drives from  $\theta$  to  $-\theta$ . Therefore, we can prove non-reciprocal transmission by studying the probe field from the CW port with various  $\theta$  in the following experiments. Two drives and probe pulses (duration of  $\tau_p = 10\mu\text{s}$ ) are sent into the system; thus, the transient bosonic excitation transportation under the synthetic gauge field can be experimentally investigated. As depicted in Fig. 2a, the amplitudes of  $a_{\text{cw}}$ ,  $a_{\text{ccw}}$  and  $m$  are separately detected. The optical outputs are instantly and simultaneously measured since their lifetimes are relatively low

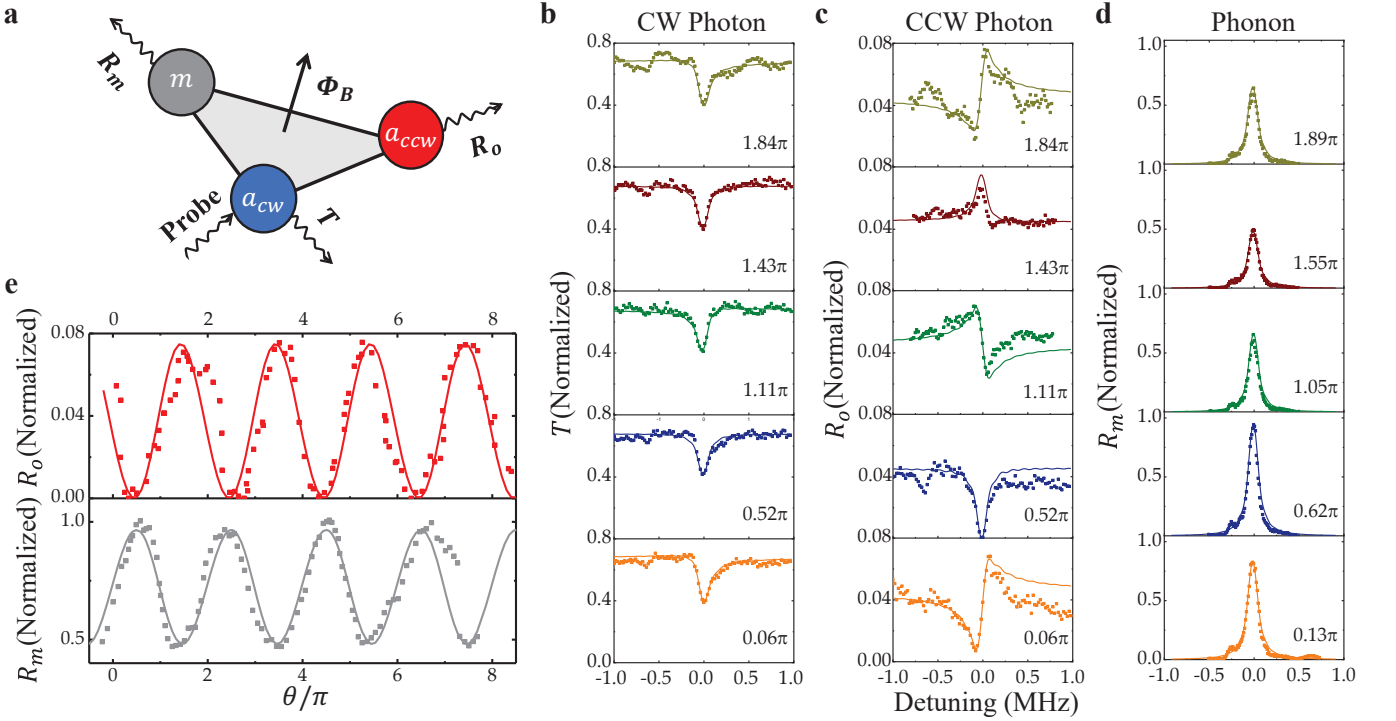


FIG. 2. **The typical photon-photon conversion and photon-phonon conversion modulated by the synthetic magnetic flux.** **a** Schematic of the mode conversions of the CW optical mode, CCW optical mode, and mechanical mode modulated by the synthetic magnetic flux. **b,c** The spectra of the CW emission mode conversion ( $R_o$ ) with the synthetic magnetic flux at  $\theta = 0.06\pi, 0.52\pi, 1.11\pi, 1.43\pi, 1.84\pi$ . The incident driving powers are 3.7 mW (CW) and 1.6 mw (CCW). The dots are the experimental results. The solid lines are the results of calculations using the parameters  $\omega_m/2\pi = 98.72$  MHz,  $\kappa_o/2\pi = 5$  MHz,  $\kappa_e/2\pi = 36$  MHz,  $\gamma_m/2\pi = 92$  kHz,  $J/2\pi = 5.3$  MHz,  $G_{cw}/2\pi = 0.6$  MHz, and  $G_{ccw}/2\pi = 0.4$  MHz, respectively. The relative optical emission power spectra of  $T$  and  $R_o$  are calculated at 10th  $\mu s$ . **d** The photon-phonon conversion ( $R_m$ ) with the synthetic magnetic flux at  $\theta = 0.13\pi, 0.62\pi, 1.05\pi, 1.55\pi, 1.89\pi$ . The relative phonon power density is measured at 12th  $\mu s$ . The corresponding parameters are  $G_{cw}/2\pi = 0.53$  MHz, and  $G_{ccw}/2\pi = 0.38$  MHz, respectively. The optomechanical coupling rate of the read laser is  $G_{cw}^{Read}/2\pi = 0.21$  MHz. The other parameters are the same as in **b**. **e**  $R_o$  and  $R_m$  at  $\delta = 0$  are related to the synthetic magnetic flux.  $R_o$  is nearly maximum when  $R_m$  is minimum. The red dots and grey dots are the experimental results of the CW to CCW optical mode conversion and photon-phonon conversion, respectively. The solid red line and solid grey line are the simulation results of these conversions, respectively. The probe propagates in the CW direction.

compared to mechanical mode, and the CW and CCW outputs are separated in the forward and backward directions. To probe the mechanical excitation, we introduce another read pulse with a duration of  $5\mu s$  at the same frequency of the drives, which arrives  $2\mu s$  after the drives [20]. Because of the longer lifetime of the phonons, the excited phonons during the first pulses can be converted into photons and measured with a time gate detection to obtain the displacement power spectral density of the mechanical mode (see Supplementary Materials).

Figures 2b-e summarize the experimental results of the system with a static synthetic gauge field ( $\theta$ ). In Figs. 2b-d, the intensities of the CW and CCW photons and the phonons for different input probe detunings are presented. For all of the spectra, we observe a significant change in the spectral shape due to the variation of  $\theta$ , with all the other experimental conditions being fixed. Such a phase-dependent response of the coupled three-

mode system manifests the synthetic gauge field, since the conversions from the CW probe to CCW photon and phonon modes are effectively manipulated, which resembles the dynamics of charged particles in a magnetic field. The CW population contains both the direct emission of the probe field and the weak indirect conversion from other modes of the closed loop, only the latter part of which is related to the phase. Therefore, the spectra are slightly modified by the synthetic gauge field  $\theta$ .

We further summarize the derived photon and phonon populations from the spectra in Fig. 2e. By varying  $\theta$  over a range of  $7\pi$ , we find the mode populations of a periodic oscillation with a period of  $2\pi$ , which means the phase dependence is repeatable and further confirms the nature of the gauge field. Since the CW photons and phonons exhibit a complementary oscillation, the conversion efficiency between the nodes in the loop-path of the three modes can be fine-tuned. The breaking of time-reversal

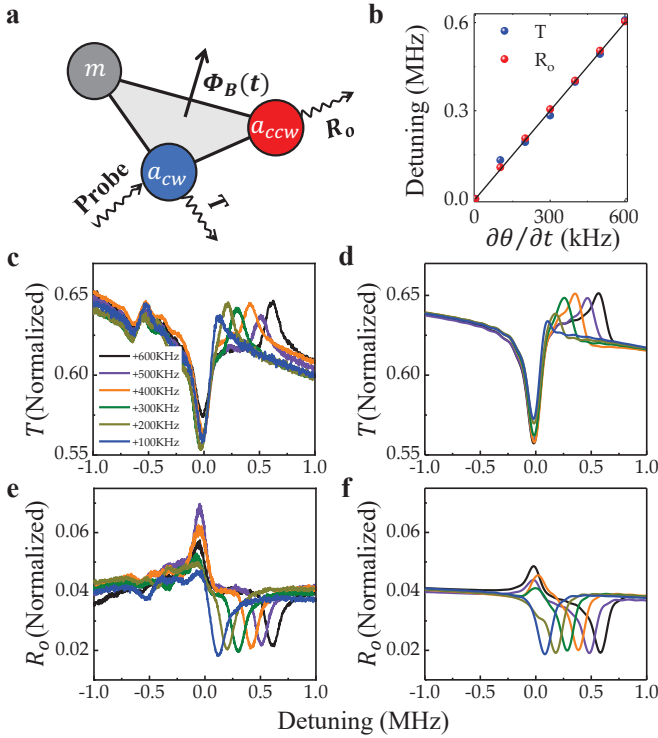


FIG. 3. **a** Schematic of the non-reciprocal emission power spectra of  $T$  and  $R_o$  under a dynamic synthetic magnetic flux. **b** Frequency detuning of  $T$  and  $R_o$  with error bars under a dynamic synthetic magnetic flux. **c-f** The non-reciprocal emission power spectra of  $T$  and  $R_o$  with a dynamic synthetic magnetic flux  $\partial\theta(t)/\partial t$  from  $+100\text{kHz}$  to  $+600\text{kHz}$ . The experimental results are shown in **c** and **e**, and the corresponding simulation results are shown in **d** and **f**, respectively. The corresponding parameters are  $G_{cw}/2\pi = 0.69$  MHz and  $G_{ccw}/2\pi = 0.31$  MHz. The other parameters are the same as in **2b**.

symmetry is also an important consequence of the synthetic gauge field. Therefore, the system should show different responses when changing  $\theta$  to  $2n\pi - \theta$ , with  $n$  being an arbitrary integer. Such breaking of the time-reversal symmetry is obvious in Fig. 2c, and the most remarkable difference can be found at  $\theta = 0.5\pi$  and  $2\pi - \theta$ . Additionally, according to the symmetry under  $\theta \rightarrow -\theta$  and  $\text{CW} \rightarrow \text{CCW}$ , for a non-zero fixed  $\theta$  that corresponds to broken time-reversal symmetry and broken parity symmetry, non-reciprocal bosonic transportation is most significant when  $\theta = 0.5\pi + 2n\pi$  with the probe laser conversion from the CW direction to the CCW direction.

The observed phase dependence and broken time-reversal symmetry of the bosonic excitation conversion in our system verify the static synthetic gauge field. Compared with a magnetic field, the synthetic gauge field has the advantages of a large dynamic range and ultra-fast tuning; thus, it provides a unique route to study the dynamics under a fast-varying gauge field [24, 25]. As an example, we study the system response with a linearly

varying gauge field  $\Phi_B(t)$ , as illustrated in Fig. 3a. For various synthetic gauge fields  $\partial\theta(t)/\partial t$  at a few hundred kHz, we observe a peak in the spectra of  $T$ , which is off-resonant with the mechanical mode. Similarly, an extra dip can be observed in the spectra of  $R_o$  when compared with Fig. 2c, and the detuning approximately  $\Delta \approx \partial\theta(t)/\partial t$ . Figures 3d and f show the theoretically calculated spectra, which agree with the experimental results. Such dynamics under a temporally varying  $\Phi_B(t)$  can be interpreted in the frequency domain, as the frequency of the CW drive is detuned with respect to the CCW drive by  $\partial\theta(t)/\partial t$ . Therefore, the induced CW photon-phonon conversion is slightly shifted from the resonance by  $\partial\theta(t)/\partial t$  and introduces a modification to the spectra at the detuning. In Fig. 3b, the extracted frequency of the varying gauge-field-induced peak or dip is plotted, which shows excellent agreement with  $\partial\theta(t)/\partial t$ . The results demonstrate the potential of our synthetic gauge field to study more complex time-dependent gauge fields [24, 25], as an arbitrary adjustable  $\Phi_B(t)$  can be realized in our system by employing arbitrary wave generators for the RF AOM inputs.

By exploiting the virtual photon and phonon degrees of freedom (DOFs) in an optomechanical resonator, coherent coupling between the modes can be achieved by external driving lasers, without requiring photonic and phononic device fabrication. Beyond the simplest three-mode model, our demonstration can be scaled to more modes in such a single resonator. Benefiting from the enhanced nonlinear optical effects due to the high quality factor and small mode volume, such as four-wave mixing [26] and Brillouin scattering [27], we could generalize the synthetic gauge field to higher virtual dimensions. Therefore, a single resonator is sufficient for studying interesting topological physics in high dimensions and is feasible for manipulating photons with unprecedented abilities. Additionally, nonlinear optical and optomechanical effects enable the generation of entangled bosonic excitations, which has potential for realizing topologically protected quantum squeezing [28], entanglement [29] and one-way quantum steering [30].

### Acknowledgments

The authors thank Xiang Xi for discussions. This work was supported by the National Key Research and Development (R&D) Program of China (grant 2016YFA0301303), the National Natural Science Foundation of China (grants 11722436 and 11704370, 11874342, 61805229), and Anhui Initiative in Quantum Information Technologies (grant AHY130200). This work was partially carried out at the USTC Center for Micro and Nanoscale Research and Fabrication.

### Author contributions

Y. C., Y.-L. Z. and Z.S. contributed equally to this work. Y.-L. Z., Z.S. C.-L.Z. and C.-H. D. conceived and de-

signed the experiment. Y.C., Z.S. and C.H.D. prepared the samples, built the experimental setup and carried out experiment measurements. Y.-L.Z. and C.-L.Z. provided theoretical support and analysed the data. C.-H.D. and C.-L.Z. wrote the manuscript with inputs from all authors. C.-H.D, C.-L.Z. and G.-C.G. supervised the project. All authors contributed extensively to the work presented in this paper.

### Additional information

Supplementary information is available in the online version of the paper. Reprints and permissions information is available online at [www.nature.com/reprints](http://www.nature.com/reprints). Correspondence and requests for materials should be addressed to C.-L.Z. ([clzou321@ustc.edu.cn](mailto:clzou321@ustc.edu.cn)) or C.-H.D. ([chunhua@ustc.edu.cn](mailto:chunhua@ustc.edu.cn)).

### Competing financial interests

The authors declare no competing interests.

---

\* †These authors contributed equally to this work.

- [1] M. Aidelsburger, S. Nascimbene, and N. Goldman, “Artificial gauge fields in materials and engineered systems,” *Comptes Rendus Physique* **19**, 394 (2018).
- [2] D. Hey and E. Li, “Advances in synthetic gauge fields for light through dynamic modulation,” *Royal Society Open Science* **5**, 172447 (2018).
- [3] N. Goldman, G. Juzeliūnas, P. ?hberg, and I. B. Spielman, “Light-induced gauge fields for ultracold atoms,” *Reports on Progress in Physics* **77**, 126401 (2014).
- [4] N. Goldman, J. C. Budich, and P. Zoller, “Topological quantum matter with ultracold gases in optical lattices,” *Nature Physics* **12**, 639 (2016).
- [5] M. Hafezi, S. Mittal, J. Fan, A. Migdall, and J. M. Taylor, “Imaging topological edge states in silicon photonics,” *Nature Photonics* **7**, 1001 (2013).
- [6] S. Mittal, E. A. Goldschmidt, and M. Hafezi, “A topological source of quantum light,” *Nature* **561**, 502 (2018).
- [7] M. V. Berry, “Quantal phase factors accompanying adiabatic changes,” *Proceedings of the Royal Society A: Mathematical, Physical and Engineering Sciences* **392**, C5 (1984).
- [8] T. Ozawa, H. M. Price, A. Amo, N. Goldman, M. Hafezi, L. Lu, M. C. Rechtsman, D. Schuster, J. Simon, O. Zeitler, and I. Carusotto, “Topological photonics,” *Reviews of Modern Physics* **91** (2019), 10.1103/revmodphys.91.011001.
- [9] G. Ma, M. Xiao, and C. T. Chan, “Topological phases in acoustic and mechanical systems,” *Nature Reviews Physics* **1**, 281 (2019).
- [10] B. M. Anderson, R. Ma, C. Owens, D. I. Schuster, and J. Simon, “Engineering topological many-body materials in microwave cavity arrays,” *Physical Review X* **6**, 041043 (2016).
- [11] P. Roushan, C. Neill, A. Megrant, Y. Chen, R. Babush, R. Barends, B. Campbell, Z. Chen, B. Chiaro, A. Dunsworth, A. Fowler, E. Jeffrey, J. Kelly, E. Lucero, J. Mutus, P. J. J. O’Malley, M. Neeley, C. Quintana, D. Sank, A. Vainsencher, J. Wenner, T. White, E. Kapit, H. Neven, and J. Martinis, “Chiral ground-state currents of interacting photons in a synthetic magnetic field,” *Nature Physics* **13**, 146 (2017).
- [12] N. A. Estep, D. L. Sounas, J. Soric, and A. Alù, “Magnetic-free non-reciprocity and isolation based on parametrically modulated coupled-resonator loops,” *Nature Physics* **10**, 923 (2014).
- [13] M. Schmidt, S. Kessler, V. Peano, O. Painter, and F. Marquardt, “Optomechanical creation of magnetic fields for photons on a lattice,” *Optica* **2**, 635 (2015).
- [14] K. Fang, J. Luo, A. Metelmann, M. H. Matheny, F. Marquardt, A. A. Clerk, and O. Painter, “Generalized non-reciprocity in an optomechanical circuit via synthetic magnetism and reservoir engineering,” *Nature Physics* **13**, 465 (2017).
- [15] N. R. Bernier, L. D. Tóth, A. Koottandavida, M. A. Ioannou, D. Malz, A. Nunnenkamp, A. K. Feofanov, and T. J. Kippenberg, “Nonreciprocal reconfigurable microwave optomechanical circuit,” *Nature Communications* **8** (2017), 10.1038/s41467-017-00447-1.
- [16] T. J. Kippenberg and K. J. Vahala, “Cavity optomechanics,” *Optics Express* **15**, 17172 (2007).
- [17] Y.-S. Park and H. Wang, “Resolved-sideband and cryogenic cooling of an optomechanical resonator,” *Nature Physics* **5**, 489 (2009).
- [18] S. Weis, R. Rivière, S. Deléglise, E. Gavartin, O. Arcizet, A. Schliesser, and T. J. Kippenberg, “Optomechanically induced transparency,” *Science* **330**, 1520 (2010).
- [19] A. H. Safavi-Naeini, T. P. M. Alegre, J. Chan, M. Eichenfield, M. Winger, Q. Lin, J. T. Hill, D. E. Chang, and O. Painter, “Electromagnetically induced transparency and slow light with optomechanics,” *Nature* **472**, 69 (2011).
- [20] C. Dong, V. Fiore, M. C. Kuzyk, and H. Wang, “Optomechanical dark mode,” *Science (New York, N.Y.)* **338**, 1609 (2012).
- [21] Y.-L. Zhang, C.-H. Dong, C.-L. Zou, X.-B. Zou, Y.-D. Wang, and G.-C. Guo, “Optomechanical devices based on traveling-wave microresonators,” *Physical Review A* **95** (2017), 10.1103/physreva.95.043815.
- [22] T. J. Kippenberg, S. M. Spillane, and K. J. Vahala, “Modal coupling in traveling-wave resonators,” *Optics Letters* **27**, 1669 (2002).
- [23] Z. Shen, Y.-L. Zhang, Y. Chen, C.-L. Zou, Y.-F. Xiao, X.-B. Zou, F.-W. Sun, G.-C. Guo, and C.-H. Dong, “Experimental realization of optomechanically induced non-reciprocity,” *Nature Photonics* **10**, 657 (2016).
- [24] D. Singlet and G. Megas, “The covariant, time-dependent aharonov–bohm effect,” *Physics Letters B* **723**, 241 (2013).
- [25] J. Jing, Y.-F. Zhang, K. Wang, Z.-W. Long, and S.-H. Dong, “On the time-dependent aharonov–bohm effect,” *Physics Letters B* **774**, 87 (2017).
- [26] A. L. Gaeta, M. Lipson, and T. J. Kippenberg, “Photonic-chip-based frequency combs,” *Nature Photonics* **13**, 158 (2019).
- [27] C.-H. Dong, Z. Shen, C.-L. Zou, Y.-L. Zhang, W. Fu, and G.-C. Guo, “Brillouin-scattering-induced transparency and non-reciprocal light storage,” *Nature Communications* **6**, 6193 (2015).
- [28] V. Peano, M. Houde, F. Marquardt, and A. A. Clerk, “Topological quantum fluctuations and traveling wave amplifiers,” *Phys. Rev. X* **6**, 041026 (2016).
- [29] A. Blanco-Redondo, B. Bell, D. Oren, B. J. Eggleton, and M. Segev, “Topological protection of biphoton

- states,” *Science* **362**, 568 (2018).
- [30] D. Cavalcanti and P. Skrzypczyk, “Quantum steering: a review with focus on semidefinite programming,” *Reports on Progress in Physics* **80**, 024001 (2017).